Kinetic models for the coordinated stepping of cytoplasmic dynein

Denis Tsygankov, Adrian W. R. Serohijos, Nikolay V. Dokholyan, and Timothy C. Elston

Citation: J. Chem. Phys. **130**, 025101 (2009); doi: 10.1063/1.3050098
View online: http://dx.doi.org/10.1063/1.3050098
View Table of Contents: http://jcp.aip.org/resource/1/JCPSA6/v130/i2
Published by the American Institute of Physics.

Kinetic models for the coordinated stepping of cytoplasmic dynein

Denis Tsygankov,[1,a] Adrian W. R. Serohijos,[2] Nikolay V. Dokholyan,[3] and Timothy C. Elston[1,b]
[1]*Department of Pharmacology, University of North Carolina at Chapel Hill, Chapel Hill, North Carolina 27599, USA*
[2]*Department of Physics and Astronomy, University of North Carolina at Chapel Hill, Chapel Hill, North Carolina 27599, USA*
[3]*Department of Biochemistry and Biophysics, University of North Carolina at Chapel Hill, Chapel Hill, North Carolina 27599, USA*

(Received 17 September 2008; accepted 17 November 2008; published online 12 January 2009)

To generate processive motion along a polymer track requires that motor proteins couple their ATP hydrolysis cycle with conformational changes in their structural subunits. Numerous experimental and theoretical efforts have been devoted to establishing how this chemomechanical coupling occurs. However, most processive motors function as dimers. Therefore a full understanding of the motor's performance also requires knowledge of the coordination between the chemomechanical cycles of the two heads. We consider a general two-headed model for cytoplasmic dynein that is built from experimental measurements on the chemomechanical states of monomeric dynein. We explore different possible scenarios of coordination that simultaneously satisfy two main requirements of the dimeric protein: high processivity (long run length) and high motor velocity (fast ATP turnover). To demonstrate the interplay between these requirements and the necessity for coordination, we first develop and analyze a simple mechanical model for the force-induced stepping in the absence of ATP. Next we use a simplified model of dimeric dynein's chemomechanical cycle to establish the kinetic rules that must be satisfied for the model to be consistent with recent data for the motor's performance from single molecule experiments. Finally, we use the results of these investigations to develop a full model for dimeric dynein's chemomechanical cycle and analyze this model to make experimentally testable predictions. [DOI: 10.1063/1.3050098]

I. INTRODUCTION

Cytoplasmic dynein is a microtubule (MT)-based motor protein involved in many intracellular processes including the directed transport of organelles and vesicles, the maintenance of the Golgi bodies, and mitosis. The motor protein is a multisubunit complex composed of two heavy chains. Each heavy chain consists of a motor domain that hydrolyzes ATP and is the putative force-generating unit, a tail that binds to the cargo and interacts with the tail of a second dynein subunit to form a homodimer and a stalk that binds to the MT [Fig. 1(a)]. Several structural studies have shown that the dynein motor domain consists of six concatenated ATPases associated with diverse cellular activities (AAA+) subunits and a C-terminal domain that is twice the size of an AAA+ subunit.[1–3] Although dynein has four ATP-binding regions, the primary hydrolytic site is located between the AAA1 and AAA2 subunits.[4–7]

In contrast to other cytoskeletal motors, such as kinesin and myosin, the mechanochemical cycle that drives dynein's unidirectional motion or the biophysical mechanisms that coordinate the motion of the two heads is less understood. Based on the results of MT binding experiments for dynein monomers,[8] Imamula *et al.* suggested a model in which the hydrolysis of ATP is tightly coupled to interactions with the MT. The model consists of the following steps. The empty (nucleotide-free) head strongly interacts with the MT. The binding of an ATP molecule stimulates the dissociation of the head from the MT (or weak association) and generates a conformational change in which the protein adopts a prepower-stroke configuration (recovery). After ATP is hydrolyzed, this free (or weakly bound) head releases the inorganic phosphate, binds strongly to the MT, and undergoes a conformational change (power stroke) to the postpower-stroke state. The details and the order of these intermediate biomechanical states were not established by these experiments, although the authors reasonably argue that the power stroke should occur while the head with ADP is strongly bound to the MT. Finally, the release of ADP completes the cycle. These considerations lead to the full chemomechanical reaction cycle shown in Fig. 1(b) (the corresponding transition rates are presented in Sec. II). The prestroke and poststroke states are indicated schematically by the "bent" (or "closed") and "straight" (or "open") dynein heads, respectively, while strong association with MT is depicted by the motor-MT complex.

We investigate coordination schemes for the two heads

[a]Electronic mail: dtsygank@med.unc.edu.
[b]Author to whom correspondence should be addressed. Present address: Department of Pharmacology, University of North Carolina, Campus Box 7365, Chapel Hill, NC 27599. Tel.: (919) 843-7670. FAX: (919) 966-5640. Electronic mail: telston@amath.unc.edu.

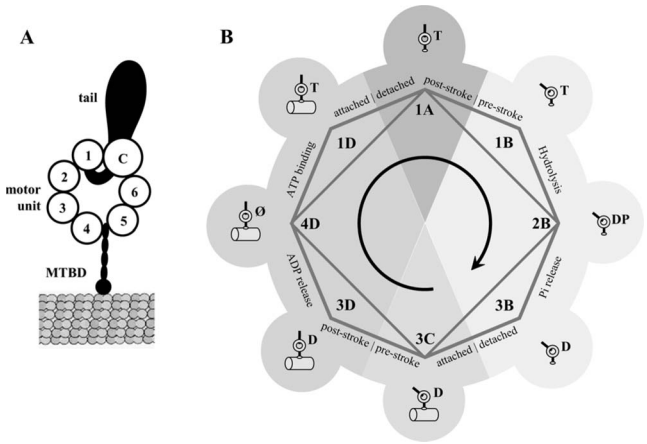

FIG. 1. The chemomechanical cycle of dynein. (a) A schematic of a single dynein head. The protein consists of a tail, a nucleotide binding motor unit, and a microtubule-binding domain (MTBD). Individual AAA+ units are numbered sequentially from 1 to 6. (b) The eight-state chemomechanical cycle of a single dynein head (octagon). The cycle consists of four biochemical transitions (ATP binding, hydrolysis, Pi release, and ADP release) and four mechanical transitions corresponding to the pre-/postpower-stroke and attachment/detachment cycles. Biochemical states are labeled by the numbers 1 to 4, and the mechanical states are labeled by the letters *A* to *D*. The square connects the distinct chemomechanical states. Intermediate states also are depicted in the diagram.

and suggest detailed models for their coupled behavior that are consistent with available data for the biochemical rate constants and other experimentally measurable quantities, such as the motor's velocity and run length. First, we construct a general interconnected graph (network) of all possible chemomechanical states of the two heads.[9] Using this graph we explore all possible chemomechanical cycles through the state space and establish conditions for the dominance of each cycle in the network. The main constraint that we impose on our model is that it should simultaneously satisfy both the high speed and high processivity of the motor.[10] We demonstrate that this constraint dictates the need for coordination between the two heads. That is, a model in which the heads work independently cannot account for both characteristics of dynein.

Our analysis resulted in the chemomechanical pathway consisting of 8 dominant states from a total of 36 states (Fig. 7). This pathway was deduced using experimental measurements to place performance constrains on the model. The currently available experimental data are not sufficient to constrain the model to a single dominant cycle through six states. In particular, there are two potential branch points in the pathway: (1) recovery of the free head can occur before or after the bound head executes the power and (2) ATP hydrolysis in the free head can occur before or after the bound head executes the power stroke. Therefore our analysis suggests which part of the pathway needs to be targeted by new experiments to determine if dynein's motion is restricted to a dominant mechanochemical cycle or if the motor uses multiple branches of the pathway.

Although understanding the biophysical interactions responsible for coordinating the two heads of dimeric dynein is an important goal, our model is not built on any *a priori* assumptions about a specific mechanism. Rather we postpone the discussion of a potential mechanism for head coordination until after analyzing the kinetic network for the ATP hydrolysis cycle of dimeric dynein. This analysis points to the biochemical steps that are the likely targets of coordination, and therefore provides insight into the mechanism of coordination.

Because our general mathematical framework is applicable to any kinetic model of a chemomechanical cycle, it should be of interest to researchers studying other motor proteins. However, the proposed mechanisms of coordination are based on unique structural features of dynein, and therefore are specific to this motor. Indeed, because of the relatively small size of kinesin's and myosin's heads, both motors bind to the MT with their heads spatially separated, so that coordination between the heads is possible only by the transmission of mechanical stress through the neck linkers. In contrast, coordination of the large dynein motor domains likely occurs by their direct interaction.

In Sec. II we summarize the currently available experimental data for dynein. This is followed by an analysis of the simple case of force-induced stepping in the absence of ATP. This model demonstrates the trade-off between high speed and high processivity. We then consider increasingly detailed models for the chemomechanical cycle of dimeric dynein and use these models to investigate mechanisms of coordination between the two heads. Finally we use the models to make experimentally testable predictions.

II. SUMMARY OF EXPERIMENTAL MEASUREMENTS

Studies on both cytoplasmic and axonemal dynein have identified the individual states in the chemomechanical cycle of dynein and the rate constants for transitions between these states. These data are summarized in Table I. We assume that the various isoforms of dynein have similar biochemical properties. The qualitative features of our results do not depend on the particular choices for the rate constants but rather on their relative values. The release of Pi following ATP hydrolysis ($2B \rightarrow 3B$) places the motor in a high activity state in which it interacts strongly with the MT ($3B \rightarrow 3C$).[11] This interaction generates a conformational change that is thought to be the force-generating step ($3C \rightarrow 3D$).[12,13] ADP release is the rate-limiting step in the chemomechanical cycle ($3D \rightarrow 4D$).[11,14] It has been shown that the motor's interaction with the MT accelerates the release of ADP in both axonemal[11] and cytoplasmic dynein,[14] which suggests that MT binding precedes ADP release.

Burgess *et al.*[15] demonstrated using negative-staining electron microscopy that axonemal dynein adopts two distinct conformations depending on its chemical state. The most notable difference between the prepower-stroke state (ADP+Vi) and the postpower-stroke state (apo) is the location of the tail relative to the motor unit. Sutoh and co-workers[13,16] verified that indeed the tail undergoes at least two ATP-dependent movements relative to the head. One transition occurs in the ATP-bound state ($1A \leftrightarrow 1B$) and another in the ADP-bound state ($3C \leftrightarrow 3D$). The kinetic rates corresponding to these tail movements have been measured[12] and are given in Table I. In another study by the same group,

TABLE I. Summary of experimental measurements for the eight-state chemomechanical cycle of dynein.

S[a]	Transition[b]	Description	Parameter name	Parameter value	Experimental value (I[c])	Source (Ref.)
	MT-D+ATP→MT-D-ATP					
	$4D \rightarrow 1D$	ATP binding	$u_{4D\rightarrow 1D}$	4.7×10^{6}/ms	4.7×10^{6}/ms (A)	31
1	$1D \rightarrow 4D$	ATP release	$w_{1D\rightarrow 4D}$	0.15/s	0.1/s (A)	32
	MT-D-ATP→MT+D^{+}-ATP					
	$1D \rightarrow 1A$	(D-ATP) detachment from MT	$u_{1D\rightarrow 1A}$		460/s (C)	8
2	$1A \rightarrow 1D$	(D-ATP) attachment to MT	$w_{1A\rightarrow 1D}$			
	MT+D^{+}-ATP→MT+D^{*}-ATP					
	$1A \rightarrow 1B$	Tail swing to prestroke	$u_{1A\rightarrow 1B}$	180/s	180[d]/s (C)	12
3	$1B \rightarrow 1A$	Tail swing to poststroke	$w_{1B\rightarrow 1A}$	4/s	4[d]/s (C)	12
	MT+D^{*}-ATP→MT+D^{*}-ADP-Pi					
	$1B \rightarrow 2B$	ATP hydrolysis	$u_{1B\rightarrow 2B}$	100/s	55/s (A) 130–150/s (A)	33, 34
4	$2B \rightarrow 1B$	ATP synthesis	$w_{2B\rightarrow 1B}$	15/s	3.5/s (A), 10/s (A), 30/s (A)	32, 33, 35
	MT+D^{*}-ADP-Pi→MT+D^{*}-ADP+Pi					
	$2B \rightarrow 3B$	Pi release	$u_{2B\rightarrow 3B}$	75/s		
5	$3B \rightarrow 2B$	Pi binding	$w_{3B\rightarrow 2B}$	8×10^{3}/ms	8×10^{3}/ms (A)	36
	MT+D^{*}-ADP→MT-D^{*}-ADP					
	$3B \rightarrow 3C$	(D^{*}-ADP) attachment to MT	$u_{3B\rightarrow 3C}$			
6	$3C \rightarrow 3B$	(D^{*}-ADP) detachment from MT	$w_{3C\rightarrow 3B}$			
	MT-D^{*}-ADP→MT-D-ADP					
	$3C \rightarrow 3D$	Tail swing to poststroke	$u_{3C\rightarrow 3D}$	0.2/s	~0.2/s (C), 150/s (A)	11, 12
7	$3D \rightarrow 3C$	Tail swing to prestroke	$w_{3D\rightarrow 3C}$	0.001/s		
	MT-D-ADP→MT-D+ADP				0.035–0.06/s; 0.006/s (w/o MT) (C), 48.2; 9.1 (w/MT) (C), 0.004 to ~1000 from (M.D.ADP) (A)	
	$3D \rightarrow 4D$	ADP release	$u_{3D\rightarrow 4D}$	0.01/s		11, 14, 37
8	$4D \rightarrow 3D$	ADP binding	$w_{4D\rightarrow 3D}$	1.5×10^{5}/ms		

[a]Mechanical state.
[b]Putative dynein conformation. D^{*}, poststroke conformation; D^{+} and D, prestroke conformation.
[c]Dynein isoform. A denotes experimental studies on axonemal dynein while C are studies on cytoplasmic dynein.
[d]To estimate this rate, the states D^{*}-ATP, D^{*}-ADP-Pi, and D^{*}-ADP were grouped as a single kinetic state.

the coordination of the tail swings of the two heads with the association/dissociation rates for the interaction between the stalk and the MT was analyzed.[8] This investigation revealed that in the postpower-stroke conformation, dynein binds strongly to the MT while in the prepower-stroke conformation the motor binds weakly to the MT.

While the primary hydrolytic site of the motor unit resides in the first *P* loop of the AAA1 subunit,[5,6] other nucleotide binding regions, such as those found in AAA2–AAA4, have been shown to play regulatory roles.[4,7,17–19] In particular, blocking nucleotide binding at AAA3 through mutagenesis of its Walker A motif produced tighter binding to the MT and diminished MT-stimulated ATPase activity.[4,7,17] Recently, Cho *et al.* showed that although ATP hydrolysis at sites AAA3 and AAA4 are not required for processivity, these sites regulate dynein's run length.[18] Abolition of hydrolysis at AAA3 slightly decreased run length, whereas blocking hydrolysis at AAA4 increased processivity. In the models described below, we suggest a mechanism for how ATP hydrolyses at these secondary sites might modulate dynein's behavior.

Single molecule experiments have begun to reveal the stepping mechanism of cytoplasmic dynein. Mallik *et al.*[20] reported that under no load conditions, dynein predominantly moves with steps of 24–32 nm, but under increasing loads of up to ~1 pN, the step size progressively decreases to 8.2 nm. These observations led the authors to suggest that dynein contains a gearing mechanism that allows it to move efficiently at high loads. However, another single molecule study found that under no load conditions, dynein predominantly takes 8.2 nm steps with occasional backstepping.[21] In yet another study, this time on yeast, Reck-Peterson *et al.*[10] showed that although 8.2 nm is the dominant step size, dynein also exhibits much larger step sizes and steps backward roughly 20% of the time at zero load. The two latter studies,[21,10] both reported a stall force of ~7 pN. In the work presented here, we take the step size of dynein to be 8.2 nm, but extension of the models to allow for larger steps and the possible biological implications of variable step sizes are presented in Sec. VII.

Single molecule experiments also have been used to estimate cytoplasmic dynein's velocity and run length. The reported velocities are 800,[21] ~500,[22] ~1000,[23–25] and 85 nm/s.[10] Reported run lengths are 1.9,[10] 0.9,[26] ~1,[25] and 0.45 μm.[22] These observations show that cytoplasmic dynein exhibit both high speed and high processivity. As target values in our simulations, we chose the smaller estimates for the velocity and run length (80 nm/s and 0.45 μm, respectively). The rationale for choosing lower bounds for these values was to establish the minimal requirements for coordination. One function of additional regulatory elements, such as auxiliary proteins or additional ATP-binding sites, may be

to enhance coordination between the heads, thereby increasing the velocity and/or run length. But even if additional regulatory elements prove not to be responsible for the higher velocities and run lengths measured under certain experimental conditions, the qualitative conclusions of our analysis remain valid. To take into account higher velocities and run lengths simply requires that the values of the two model parameters related to coordination be readjusted. Based on these considerations and the experimental measurements described above, we adopt the kinetic parameters shown in Table I.

III. FORCE-INDUCED STEPPING IN THE ABSENCE OF ATP

Recent experiments by Gennerich *et al.*[27] demonstrated that cytoplasmic dynein moves processively along MTs under sufficiently large applied loads *in the absence of ATP*. The following simple mechanokinetic model provides a possible mechanism for this force-induced stepping and allows the derivation of explicit expressions for the mean run time, run length, and velocity of the motor as functions of load.

Consider a dimeric dynein motor attached to a MT in the absence of ATP. Both heads of the motor interact strongly with the MT. Because of the asymmetry of the MT and the coupling between the two heads, the dissociation rates of the heads are not in general equal. To distinguish these rates, let k_{df} denote the dissociation rate of the front head (with respect to the minus end of the MT) and k_{db} denote the dissociation rate of the back head. Consider the case in which only one head is attached to the MT. Then there are two possibilities for where the free head can bind, in front or in the back of the attached head. Let k_{af} denote the association rate for the front site and k_{ab} denote the association rate for the back site. If the dissociation rates are much smaller than the association rates, then the probability of both heads detaching is small but finite. In the absence of an external load, the motor will slowly diffuse on the MT with large run times but zero mean velocity and run length. In this case detailed balance requires that the rates satisfy the condition $(k_{db}k_{af})/(k_{df}k_{ab})=1$. Although the intrinsic asymmetry of the MT might require that even under no load the dissociation rates for the front and the back heads are not the same (i.e., $k_{db}\neq k_{df}$) and that the association rates also are not equal (i.e., $k_{ab}\neq k_{af}$), the requirement of detailed balance still must be satisfied.

Now suppose a constant force is applied to the motor so that the horizontal component of this force, F, is in the direction of the minus end of the MT. This force can affect all the detachment and attachment rates. In this situation, the rates must satisfy the requirement

$$\frac{k'_{db}k'_{af}}{k'_{df}k'_{ab}} = e^{-F\Delta x/kT}, \tag{1}$$

where the primes denote the force-dependent rates and Δx is the step size of the motor ($\Delta x=8.2$ nm). We take the rates to have the forms

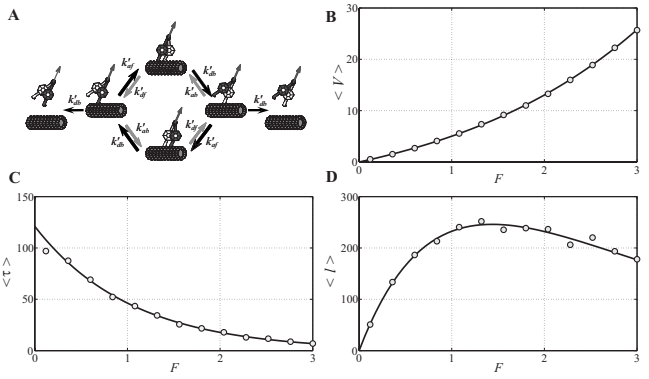

FIG. 2. (a) Schematic representation of dynein stepping in the absence of ATP. The arrows pointing from the motors indicate the direction of the applied load. (b) The mean velocity $\langle V\rangle$ as a function of the applied load F. The solid curve corresponds to Eq. (5). (c) The average run time $\langle\tau\rangle$ as a function of the applied load F. The solid curve corresponds to Eq. (3). (d) The average run length $\langle l\rangle$ as a function of the applied load F. The solid curve corresponds to Eq. (4). The dots represent the results of direct Monte Carlo simulations (each data point is an average over 500 runs).

$$k'_{db} = k_{db}\exp\left(\frac{D_1F}{k_BT}\right), \quad k'_{df} = k_{df}\exp\left(\frac{D_2F}{k_BT}\right),$$
$$k'_{ab} = k_{ab}\exp\left(-\frac{D_3F}{k_BT}\right), \quad k'_{af} = k_{af}\exp\left(-\frac{D_4F}{k_BT}\right). \tag{2}$$

Equations (1) and (2) require that the D satisfy the relationship $D_1-D_2+D_3-D_4=\Delta x$.

Mechanistic and geometric considerations suggest the following.

(1) The rear head is more strained under a forward load than the front head, effectively supporting most of the load. Thus, the force F causes the dissociation rate for this head, k'_{db}, to increase by a greater amount than the dissociation rate of the front head, k'_{df} $(D_1>D_2)$.
(2) It is more likely that under a forward load the free head binds to a site in front of the bound head than to a site behind it $(D_3>D_4)$. Otherwise, the motor performs mechanical work against the load.

Based on these considerations, we assume that the main effect of the force is to increase the rate at which the rear head detaches and decrease the rate at which a free head binds to the back site. A natural choice of parameters in this situation is D_1, $D_3\sim\frac{1}{2}\Delta x$ and D_2, $D_4\sim 0$, but our analysis is not restricted to this choice and is valid in general. Our model does not rely on but is consistent with the mechanism proposed by Reck-Peterson *et al.*[10] in which the angle between the MT and the MT binding domain (MTBD) is the parameter that links the effect of the applied force with the MT affinity of the motor heads. The resulting mechanical cycle with the corresponding rates for dynein stepping in the absence of ATP is shown in Fig. 2(a).

For the model described above, the general expressions for the mean run time $\langle\tau\rangle$, run length $\langle l\rangle$, and velocity $\langle V\rangle$ are, respectively,

$$\langle \tau \rangle = \frac{k'_{db} + k'_{df} + k'_{af} + k'_{ab}}{k'_{db}(k'_{db} + k'_{df})}, \tag{3}$$

$$\langle l \rangle = \Delta x \frac{k'_{db}k'_{af} - k'_{df}k'_{ab}}{k'_{db}(k'_{db} + k'_{df})}, \tag{4}$$

$$\langle V \rangle = \Delta x \frac{k'_{db}k'_{af} - k'_{df}k'_{ab}}{k'_{db} + k'_{df} + k'_{af} + k'_{ab}}. \tag{5}$$

The derivation of these results is given in Appendix A. General expressions for the mean velocity and diffusion in sequential models with irreversible detachments can be found in Ref. 28. Figures 2(b)–2(d) show the characteristic behavior of these three quantities as functions of the external force. Under increasing load the motor steps faster and the average velocity $\langle V \rangle$ increases [Fig. 2(b)]. However, the increased dissociation rate makes the mean run time $\langle \tau \rangle$ shorter [Fig. 2(c)]. As a result, the average run length $\langle l \rangle$ first increases and then starts to decrease monotonically to zero at large loads [Fig. 2(d)]. This behavior demonstrates the trade-off between high speed and high processivity. Importantly, this model does not take into account coordination between the heads. As we demonstrate below such coordination is required to produce the experimentally measured velocity and run length in the presence of ATP. Strictly speaking, one can consider the inequality of the zero-load rates k_{db} and k_{df} and k_{ab} and k_{af} as a type of coordination that "tells" the motor which head is leading and which is trailing. However, this kind of "asymmetry driven coordination" alone is not sufficient to produce simultaneously the large velocities and run lengths observed in the presence of ATP because the attachment and detachment steps are relatively fast compared to the rate-limiting biochemical steps. Therefore, as we show in the following sections additional coordination of the hydrolysis cycles of the two heads is required.

The situation in which the applied load acts in the opposite direction (toward the plus end of MT) is also described by the model. However, in general the parameters D_1, D_2, D_3, and D_4 again will be different for forward and backward loads because of the intrinsic asymmetry of the MT. Fitting this model to experimental data for applied loads in both the plus and minus end directions should provide valuable information about the intrinsic asymmetry of the dynein/MT interaction.

IV. A MODEL FOR TWO-HEADED DYNEIN BASED ON A FOUR-STATE ATP HYDROLYSIS CYCLE

To further demonstrate the main ideas of our analysis, we proceed to a model that combines the ATP hydrolysis cycle with motor stepping. We assume that ATP binding to the catalytic site and detachment of the stalk from the MT occur as a single step with a rate d. Similarly we combine the recovery stroke with ATP hydrolysis, phosphate release with attachment, and power stroke with ADP release. The rate constants for these steps are r, a, and p, respectively. The resulting four-state chemomechanical cycle for a single head is depicted in Fig. 1(b) as the square. At any given time a dimeric dynein motor can be in one of the 16 states. We

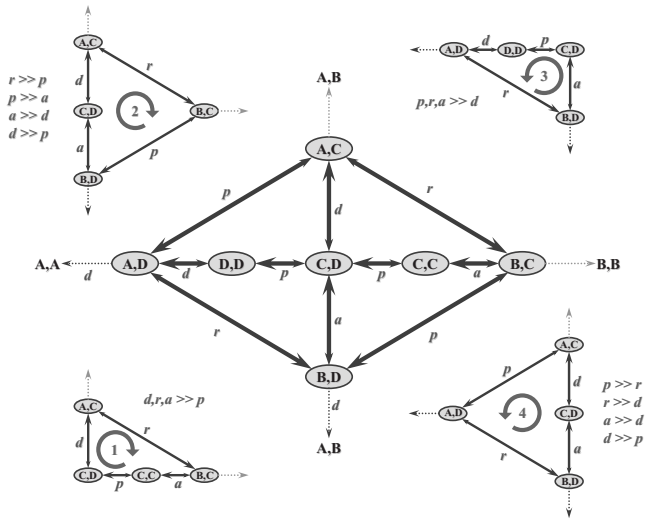

FIG. 3. A kinetic diagram of two-headed dynein model based on four chemomechanical states. The middle diagram corresponds to the seven states that compose the two-headed network when at least one head is attached to the MT. In this model, we do not distinguish states (i,j) from (j,i). When the motor reaches states $(A,\ A)$, $(A,\ B)$, and $(B,\ B)$ the motor dissociates from the MT and the run ends. The diagrams in the four corners represent the possible forward cycles. The larger arrow heads indicate the forward transitions, while the smaller arrow heads indicate the reverse transitions.

denote these states as (i,j), where the indices i and j are any of the four states depicted as A-D in Fig. 1(b). Four of the states, $(A,\ A)$, $(A,\ B)$, $(B,\ A)$, and $(B,\ B)$, correspond to a motor with both heads detached from the MT, and therefore mathematically represent absorbing states. That is, a motor transition into one of these states signifies the end of a run.

We assume that the heads are identical, and therefore consider states (i,j) and (j,i) to be indistinguishable. This symmetry assumption is true for identical *noninteracting* heads and provides a baseline to which models that contain coordination can be compared. As we demonstrate, establishing kinetic rules that generate pathway designs consistent with the motor's measured performance requires an asymmetry between the front and back heads, which results from their interaction and represents coordination. The model for the chemomechanical cycle while the motor is attached to MT consists of the seven states shown in Fig. 3. In this model the motor dissociates from the MT from either states $(A,\ D)$ and $(B,\ D)$, in which one head is detached and the other nucleotide-free head detaches upon ATP binding, or from states $(A,\ C)$ and $(B,\ C)$, through the reverse transition from (C) to (B), in which the bound head detaches from the MT upon Pi binding. While the motor is attached to the MT, the following four forward cycles are possible (see Fig. 3):

$$(C,\ D) \rightarrow (A,\ C) \rightarrow (B,\ C) \rightarrow (C,\ C),\ \text{cycle 1},$$

$$(C,\ D) \rightarrow (A,\ C) \rightarrow (B,\ C) \rightarrow (B,\ D),\ \text{cycle 2},$$

$$(C,\ D) \rightarrow (D,\ D) \rightarrow (A,\ D) \rightarrow (B,\ D),\ \text{cycle 3},$$

$$(C,\ D) \rightarrow (A,\ C) \rightarrow (A,\ D) \rightarrow (B,\ D),\ \text{cycle 4}. \tag{6}$$

The probability that the motor completes a cycle without

dissociating from the MT depends on the relative values of the rates. The first cycle is dominant when $p \ll d, r, a$. Since ADP release is believed to be the rate-limiting step, this condition is plausible and corresponds to a simple picture in which the motor spends most of the time in state (C, C) with both heads containing ADP and attached to the MT. When ADP is finally released from one of the heads, this head rapidly progresses through its chemomechanical cycle and returns to state (C) before the other head releases ADP. As a result of this behavior, the motor takes forward steps one at a time guaranteeing processivity. The problem with this condition is that it restricts the velocity of the motor. The larger p, the faster the motor moves, but if the value of d is fixed increasing p also increases the probability of dissociation, effectively shortening the run length. This situation is reminiscent of the example discussed in Sec. III and further demonstrates the trade-off between processivity and high velocities.

Because coordination between the two heads is not included in the current model, the two heads are not required to alternate steps, so that the movement along the MT consists of both head-over-head and inch worming movements. This observation contradicts experimental evidence,[21] in which it was observed that dynein performs head-over-head motion. One possibility to eliminate this discrepancy is to assume that the kinetic rates differ for the front and rear heads. For example, if we assume that ADP is released faster from the rear head than the leading head, then the motor will step mainly in a head-over-head fashion. This assumption also increases the overall motor velocity without sacrificing the length of its run.

Two experimental facts allow us to speculate on the mechanism for the coordination of the hydrolysis cycle of the two heads. First, according to the experimental results of Mizuno *et al.*,[2] a dynein head that is attached to the MT adopts a specific orientation in which the plane of the AAA ring is parallel to the MT and the AAA2 and AAA3 subdomains face forward with respect to the minus end of the MT. Second, dynein takes mostly 8.2 nm steps, while the outer diameter of its AAA rings is ~16 nm, suggesting that dynein heads form an overlapping (compact) conformation[10] when both heads are attached to the MT at adjacent sites (Fig. 4). Therefore, it is plausible that the nucleotide binding pockets of the two heads are not identical, producing asymmetric release rates.

The potential mechanism of coordination shown in Fig. 4 assumes that in states such as (C, C) or (D, D), the two heads have distinct chemomechanical properties that result from their relative position on the MT. Alternatively, the second cycle given in Eq. (6) seems to achieve alternating stepping of the heads without requiring additional assumptions about coordination. However, for this cycle to be dominant, the rates must satisfy the conditions $r \gg p$, $p \gg a$, $a \gg d$, and $d \gg p$. These conditions cannot be simultaneously satisfied, and therefore necessitate coordination between the two heads. For this case, it also is possible to propose a form of coordination that overcomes this restriction on the rates. Suppose that the rates satisfy the relations $d, r \gg p$ and $a \ll p$ when the motor is in state (B, C) but $a \gg d$ when the motor is in state (B, D). These conditions imply that the detached head does not reattach to the MT until after the attached head has performed its power stroke. Although such a mechanism agrees with the concept of a power-stroke biasing forward motion, the condition $a \gg d$ is hard to justify because attachment to the MT is coupled with the release of the phosphate group, which is a relatively slow process as compared to detachment from the MT and ATP binding. The last two cycles in Eq. (6) are conceptually identical to the two considered above but require the following hard-to-satisfy conditions: $d \ll p, r, a$ and $p \gg r$, $r \gg d$, $a \gg d$, and $d \gg p$, respectively.

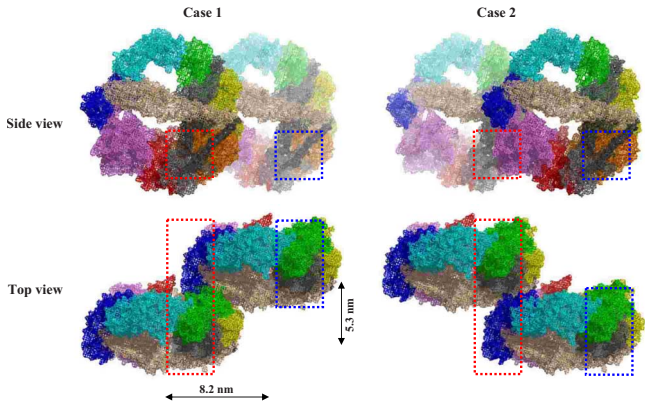

FIG. 4. (Color online) A potential structural basis for the coordination of the two dynein heads. In a hand-over-hand mechanism, there are two possibilities for stacking the motor units. The scenarios are denoted as case 1 and case 2 in the figure. Both cases assume that the two heads occupy MT binding sites separated by 8.2 nm and that the two heads rest on adjacent tubulin protofilaments, which are separated by ~5 nm. In both cases, the primary catalytic site of the rear head (marked with the left rectangle) is always "covered" by the front head, while that of the front site (right rectangle) is exposed. This observation suggests that the leading and trailing heads are not in identical chemical states and provides a mechanism for coordinating their hydrolysis cycle.

Although the four-state model for a single dynein head presented in this section does not explore the full range of possible mechanisms of coordination between the two heads, two important classes of chemomechanical cycles emerged from this analysis: (1) one-head-at-a-time motion in which coordination between the heads ensures that the back head passes through its chemomechanical cycle, while the state of the front head does not change and (2) out-of-phase motion in which coordination is used to avoid the front and back heads being in the same chemical state.

V. A MODEL FOR TWO-HEADED DYNEIN BASED ON A SIX-STATE ATP HYDROLYSIS CYCLE

To study potential mechanisms of coordination in greater detail, we expand our analysis and consider the six-state model for a single head shown in Fig. 5. Here the cycle contains all four biochemical states of the ATP hydrolysis cycle and two mechanical transitions (power stroke and recovery). Association and dissociation of the heads are coupled with the corresponding biochemical triggers: Pi release and ATP binding. The full network for the double-headed case now has 36 states and 32 distinct minimal cycles. The nine states in the top-left corner of the state

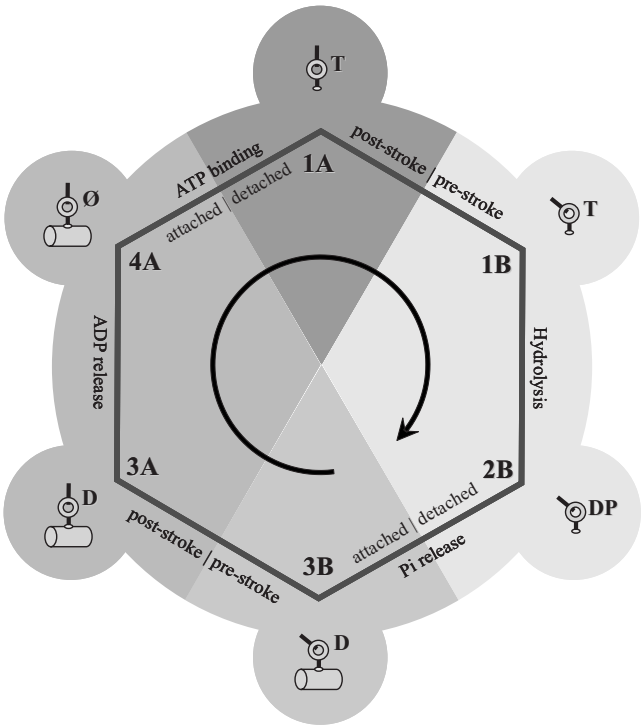

FIG. 5. A six-state chemomechanical model of dynein. In this model, there are four biochemical states of the ATP hydrolysis cycle and two mechanical transitions: prestroke to poststroke (power stroke) and poststroke to prestroke (recovery). Again the biochemical states are labeled with numbers 1 to 4, while the mechanical states are labeled with letters A and B, respectively. Each intermediate state is shown as a schematic. Attachment and detachment processes are coupled to Pi release and ATP binding, respectively.

matrix shown in Fig. 6 correspond to situations in which the motor has dissociated from the MT and represent absorbing boundaries of the network. Exclusion of these states produces 16 minimal cycles.

Under physiological conditions the $(4A)\rightarrow(1A)$ transi-

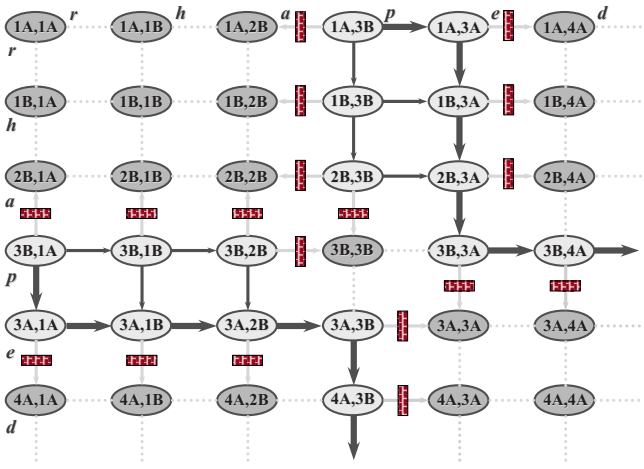

FIG. 6. (Color online) The kinetic network for dimeric dynein using the six-state model shown in Fig. 5. The rates are labeled as r for recovery, h for hydrolysis, a for attachment (coupled with Pi release), p for power stroke, e for ADP release, and d for detachment (coupled with ATP binding). Darker ovals indicate either dissociated states (top-left corner), states immediately leading to dissociation (see text), or mechanically symmetric states (bottom-right corner). Brick walls indicate the transitions that lead to these unfavorable states.

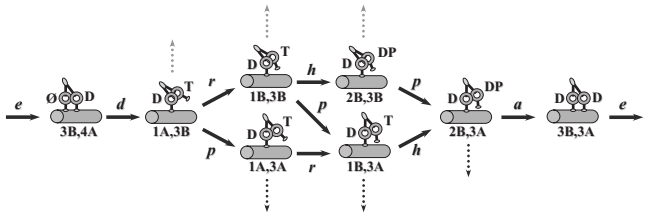

FIG. 7. Schematic representation of the "out-of-phase" scenario. There are three possible out-of-phase cycles as in Eq. (6). The dotted arrows pointing up indicate the rare dissociation events through the transition $(3B)\rightarrow(2B)$. The dotted arrows pointing down indicate the rare dissociation events that occur when one head is free and the other reaches state $(4A)$.

tion, in which one of the heads detaches from the MT, is much faster than any other transition in the cycle. Therefore, reaching the states $(1A,\ 4A)$, $(1B,\ 4A)$, $(2B,\ 4A)$ or $(4A,\ 1A)$, $(4A,\ 1B)$, $(4A,\ 2B)$ guarantees that with a high probability the next transition will lead to dissociation. Thus, for the motor to be highly processive, these states need to be "kinetically excluded" from the network (see the discussion below). The remaining network has only six minimal cycles. Two of these cycles belong to the one-head-at-a-time scenario:

$$\begin{aligned}&(1A,\ 3B)\rightarrow(1B,\ 3B)\rightarrow(2B,\ 3B)\rightarrow(3B,\ 3B)\\&\quad\rightarrow(3B,\ 3A)\rightarrow(3B,\ 4A),\ \text{cycle (1)},\\&(1A,\ 3A)\rightarrow(1B,\ 3A)\rightarrow(2B,\ 3A)\rightarrow(3B,\ 3A)\\&\quad\rightarrow(3A,\ 3A)\rightarrow(3A,\ 4A),\ \text{cycle (2)},\end{aligned}\tag{7}$$

and four belong to the out-of-phase scenario:

$$\begin{aligned}&(1A,\ 3B)\rightarrow(1A,\ 3A)\rightarrow(1B,\ 3A)\rightarrow(2B,\ 3A)\\&\quad\rightarrow(3B,\ 3A)\rightarrow(3B,\ 4A),\ \text{cycle (3)},\\&(1A,\ 3B)\rightarrow(1B,\ 3B)\rightarrow(1B,\ 3A)\rightarrow(2B,\ 3A)\\&\quad\rightarrow(3B,\ 3A)\rightarrow(3B,\ 4A),\ \text{cycle (4)},\\&(1A,\ 3B)\rightarrow(1B,\ 3B)\rightarrow(2B,\ 3B)\rightarrow(2B,\ 3A)\\&\quad\rightarrow(3B,\ 3A)\rightarrow(3B,\ 4A),\ \text{cycle (5)},\\&(1A,\ 3A)\rightarrow(1B,\ 3A)\rightarrow(2B,\ 3A)\rightarrow(3B,\ 3A)\\&\quad\rightarrow(3B,\ 4A)\rightarrow(3A,\ 4A),\ \text{cycle (6)}.\end{aligned}\tag{8}$$

Note that so far no coordination or symmetry breaking is assumed, and therefore $(i,j)\equiv(j,i)$. Moreover, the last cycle in Eq. (8) cannot be dominant in the network because as mentioned above the $(4A)\rightarrow(1A)$ transition is much faster than $(3B)\rightarrow(3A)$, and hence the state $(3A,\ 4A)$ has a low probability of being reached. The remaining three cycles are represented schematically in Fig. 7.

The states shown in Fig. 7 are the most visited in the network during progression through the cycle, but they are not exclusive. Other states in the network have low but finite probabilities of being visited. Such occasional events can serve as transition points in extended models that take into account more than one operating regime for the motor, such as the inclusion of a diffusive pathway.[29]

If the power stroke is the rate-limiting transition, then the motor follows the first minimal cycle in Eq. (7). High motor speed and head-over-head stepping require a coordination mechanism that ensures that the transitions $(3B,\ 3B)\rightarrow(3B,\ 3A)$ and $(3B,\ 3B)\rightarrow(3A,\ 3B)$ alternate from cycle to cycle. This condition is possible only if the transition corresponding to the power stroke is faster for one of the two heads, say, the leading one. If ADP release is rate limiting, then the second minimal cycle dominates the network. The mechanism of coordination in this case is the one discussed in Sec. IV [see the first cycle in Eq. (6)]. The appeal of this scenario is the simplicity of its kinetics and coordination, but the disadvantage is that it is difficult to justify the mechanically symmetric states $(iA,\ jA)$ and $(iB,\ jB)$ when $i,j>3$, i.e., when both heads are attached to the MT in the same structural form. Thus, we will focus on the second (out-of-phase) scenario.

To have the out-of-phase scenario dominate in the network, the motor has to avoid not only the states that lead to the dissociation of both heads but also the mechanically identical states on the diagonal and at the bottom-right corner of the state matrix shown in Fig. 6. The "brick walls" in this figure represent kinetically unfavorable transitions. To achieve this structure requires that

(1) $e\ll r,h,a$ to avoid dissociation,
(2) $e\gg p$ to avoid the state $(3A,\ 3A)$, and
(3) $p\gg a$ to avoid the state $(3B,\ 3B)$.

However, these conditions cannot be satisfied without assuming that the mechanochemical cycles of the two heads are coordinated. To achieve coordination, we propose the following two mechanisms.

(A) The ADP-release rate e_1 is small $(e_1\ll r,h,a)$ until the heads form a compact conformation (both heads attached to the MT 8.2 nm apart) at which point the release rate becomes $e_2\gg e_1$.
(B) The power-stroke rate $p_2\ll e_2$ when both heads are attached to MT but increases to a rate $p_1\gg a$ when the other head is free to diffuse.

Experiments on single dynein heads suggest that both rates p and e are much smaller than the other rates of the single-head cycle (see Table I). The essence of the coordination proposed above is that the second head effectively speeds up these rates under appropriate conditions (A) and (B). How fast must the rates p_1 and e_2 be to provide a mean velocity and run length in agreement with experimental values? To answer this question we plot these quantities as functions of p_1 and e_2 (Figs. 8 and 9).

Figures 8 and 9 show that experimentally plausible values for mean velocity ($\approx$80 nm/s) and mean run length ($\approx$450 nm) can be obtained if the rates p_1 and e_2 are about 500/s and 16/s, respectively. Since all other rates in the model are fixed to the values listed in Table I, once p_1 and e_2 have become sufficiently large the velocity or run length becomes independent of these parameters. This saturation effect occurs because the proposed coordination mechanism kinetically isolates particular pathways within the full network of states, but the mean characteristics of these pathways depend on all the rates of the single-headed cycle and not just those involved in the coordination. Nevertheless, it is clear that the desired values for mean velocity and mean run length require relatively high values for the regulatory rates p_1 and e_2, indicating the necessity for strong coordination.

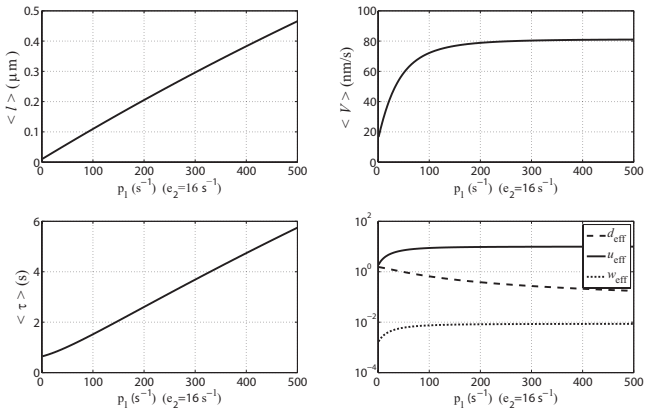

FIG. 8. Mean run length $\langle l\rangle$, mean run time $\langle\tau\rangle$, mean velocity $\langle V\rangle$, and effective rates u_{eff}, w_{eff}, and d_{eff} (described in Sec. VI) as functions of the parameter p_1 while the rate e_2 is fixed to be 16 s^{-1} and the values of the other rate constants are given in Table I.

For effective coordination in our model, it is also crucial that the rate e_1 (rate of ADP release from an attached head while the other is detached) is sufficiently small. To demonstrate this fact we plot the mean characteristics of the motor's motion as functions of this rate in Fig. 10. For the range of parameter values considered in this figure, the velocity is almost independent of e_1, while the run length and run time rapidly decrease because of an increase in the effective detachment rate (for details on effective rates see Sec. VI). We speculate that this particular rate is modulated by the ATP hydrolysis site located at AAA4. Consistent with our model, abrogation of this sited lead to a dramatic increase in dynein processivity but caused only a moderate change in the velocity.[18] It is important to note that this regulatory effect of the AAA4 site is observed only in the dimeric form of dynein and not in the monomeric form.[18] This suggests that this site primarily regulates coordination between the heads rather than the hydrolytic cycle of an individual head.

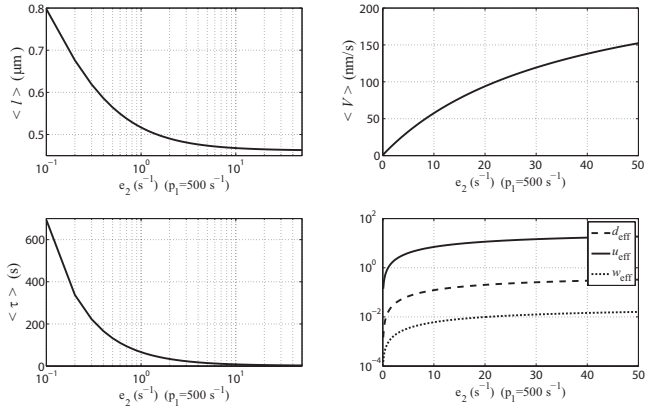

FIG. 9. Mean run length $\langle l\rangle$, mean run time $\langle\tau\rangle$, mean velocity $\langle V\rangle$, and effective rates u_{eff}, w_{eff}, and d_{eff} as functions of the parameter e_2 while the rate p_1 is fixed to be 500/s.

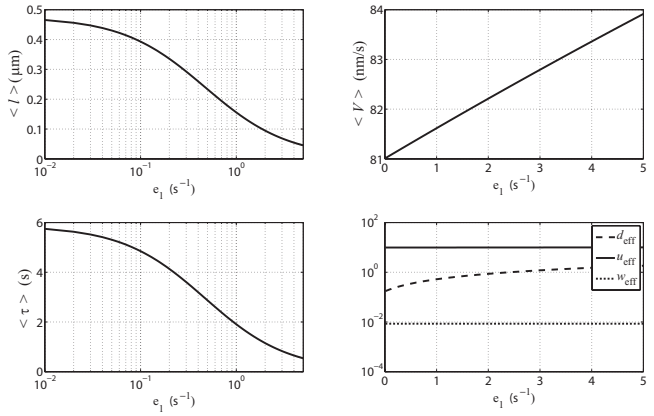

FIG. 10. Mean run length $\langle l \rangle$, mean run time $\langle \tau \rangle$, mean velocity $\langle V \rangle$, and effective rates u_{eff}, w_{eff}, and d_{eff} as functions of the parameter e_1 (the rates p_1 and e_2 are fixed at 500/s and 16/s, respectively).

In summary, we have shown that a simple coordination mechanism expressed in terms of kinetic rules for a minimal number of transition rates results in a dominant pathway through the network of motor states that generates behavior consistent with experimental observations. Notice that the parameter values characterizing the motor's coordination are conditional in the sense that if future experiments give a more accurate estimation for the transition rates, an adjustment of these parameters might be necessary to reproduce the observed values for the velocity and/or run length. However, we stress that the qualitative features of the model will remain the same as long as the relative relationships between the rates are preserved, meaning that slow transitions in the single-head cycle remain slow, while fast rates remain fast.

VI. ANALYSIS OF THE MODEL AND PREDICTIONS

A convenient way to analyze the models presented above is by looking at the effective rates of progression through the chemomechanical cycles and the effective detachment rate. The mathematical definition of these effective rates is based on the conservation of probability fluxes.[30] Consider the full set of dimeric dynein states (i,j) as a single site in an infinite chain of identical sites. Advancing from one site to the next corresponds to completing the enzymatic cycle and taking a physical step of $\Delta x = 8.2$ nm. The mean forward and backward fluxes between two adjacent sites are given by

$$\pi_f = u_{\text{eff}} T, \quad \pi_b = w_{\text{eff}} T,$$

respectively, where π_f and π_b can be explicitly expressed in terms of mean times spent at peripheral states of the site (see Appendix B for details), $T = \Sigma_{i,j} \int_0^\infty p_{i,j}(t) dt$ is the mean run time, and $p_{i,j}(t)$ is the probability to be in state (i,j) of any site at time t. Similarly, the effective detachment rate is found from

$$\pi_d = d_{\text{eff}} T.$$

Conservation of the mean fluxes requires $\pi_d = 1$, so that $d_{\text{eff}} = 1/T$.

This formalism allows a simple representation of the full model as a linear Markov chain with the effective rates easily obtainable from the master equation by inversion of a relatively low-dimensional matrix ($< N^2$). The mean run time, $\langle \tau \rangle = 1/d_{\text{eff}}$, mean run length, $\langle L \rangle = \Delta x (u_{\text{eff}} - w_{\text{eff}})/d_{\text{eff}}$, and mean velocity, $\langle V \rangle = \Delta x (u_{\text{eff}} - w_{\text{eff}})$, are easily expressed in terms of these effective rates.

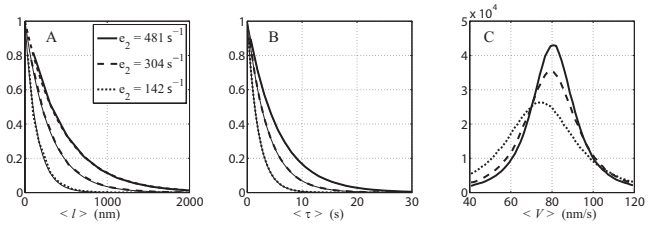

FIG. 11. Distributions of (a) run length, (b) run time, and (c) velocity for three values of the parameter e_2 obtained from Monte Carlo simulations (10^6 runs) of the linear Markov chain model using the numerically calculated effective rates (see text for details). The thin solid curves shown in (a) and (b) are exponential fits to the distributions. The run time and run length distributions are rescaled to have a maximum value of unity.

Figure 11 shows distributions for the run length, run time, and velocity for different values of e_2 (the rate of ADP release from the dynein in the compact conformation) obtained from Monte Carlo simulations of the model. Both run length and run time have exponential distributions in agreement with the analysis in Appendix B. The behavior of the corresponding mean values is shown in Fig. 9. Because we define the velocity as the ratio of run length to run time, which are correlated random variables, the velocity distribution has a non-Gaussian shape that broadens with decreasing run length [Fig. 11(c)].

Finally, we explore the effects of varying the concentration of the reactants on the motor's performance. Because the transition $3B \rightarrow 2B$ (phosphate binding) contributes directly to the dissociation of the motor, the motor run length depends strongly on the phosphate concentration [Pi]. It turns out that the velocity also is sensitive to the phosphate concentration. Figure 12 shows that the effective detachment rate initially increases rapidly and then slowly decreases, while the effective forward rate monotonically decreases, eventually becoming smaller than the effective detachment rate. As a result both the average run length and velocity decrease with increasing phosphate concentration. The average run time initially decreases as a function of [Pi] but then

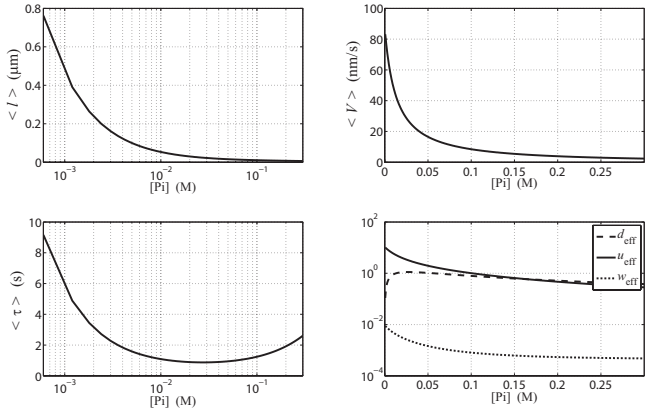

FIG. 12. Mean run length $\langle l \rangle$, mean run time $\langle \tau \rangle$, mean velocity $\langle V \rangle$, and effective rates u_{eff}, w_{eff}, and d_{eff} as functions of inorganic phosphate concentration [Pi].

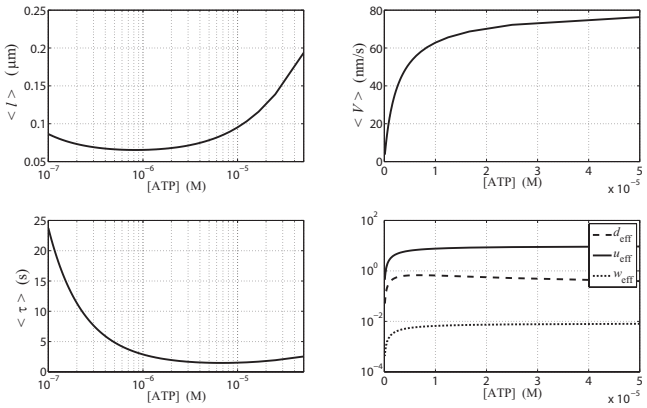

FIG. 13. Mean run length $\langle l \rangle$, mean run time $\langle \tau \rangle$, mean velocity $\langle V \rangle$, and effective rates u_{eff}, w_{eff}, and d_{eff} as functions of ATP concentration.

starts to increase. This effect is due to the motor becoming stuck at the original site until it eventually dissociates from the MT. Note that these predictions are tightly coupled to the assumption that following ATP hydrolysis, a head containing both ADP and Pi is detached from (or weakly interacts with) the MT. Current experimental results[8,14] disagree on this issue. If future experiments confirm the high sensitivity of the motor's velocity and run length on the phosphate concentration, this result would provide indirect evidence to support the scenario in which heads containing both ADP and Pi do not interact strongly with the MT.

Increasing the ADP concentration also affects the mean velocity by increasing the backward transition $4A \rightarrow 3A$, but it does *not* substantially change the run length (data not shown). The effect of varying the ATP concentration is less intuitive because the coordination mechanism in our model was constructed based on the observation that ATP binding is the fastest rate in the single-headed dynein cycle. Breaking this condition changes the effective fluxes in a nontrivial way. Figure 13 shows that similar to increasing the phosphate concentration, decreasing the ATP concentration strongly affects both the run length and velocity.

VII. DISCUSSION

Here we analyze the network of chemomechanical states that underlies the processive motion of dimeric dynein. The network was constructed from experimental measurements for the ATP hydrolysis cycle of a single head (Fig. 1). The simplest model of motor function is one in which the two dynein heads operate independently. In this case, the transition rates satisfy the relation $u_{(i,j)\rightarrow(i,j+1)}=u_{(k,j)\rightarrow(k,j+1)}$. Our analysis revealed that such a model cannot simultaneously account for dynein's large velocity and high processivity as measured using single molecule techniques. Therefore, our goal was to establish a minimal set of relationships for the rate constants that must be satisfied by kinetic models of dynein's chemomechanical cycle. That is, we sought to determine the requirements for coordination between the heads.

Because processive stepping requires that the individual dynein heads repeatedly detach and attach to the MT, there is a finite probability that both heads become detached allowing the motor to diffuse away from the MT. For this reason, in models that lack coordination between the two heads, increasing the forward transition rates generates higher motor velocities but sacrifices processivity. To illustrate this tradeoff, we considered the simple situation in which ATP is absent from the system and motor stepping is induced by an external force [Fig. 2(a)]. The magnitude and direction of the force are experimentally controllable parameters that affect the transition rates between the kinetic states. Under these conditions, the motor's velocity monotonically increases as a function of the load. However, the run length behaves nonmonotonically, reaching a maximum value at intermediate forces before asymptotically approaching zero at high loads [Figs. 2(b)–2(d)]. The nonmonotonic behavior of the run length is not unique to this simple model but would occur for other models in which the two heads operate independently. Our analysis demonstrates that to achieve both high speeds and high processivity requires coordination of the chemomechanical cycles of the two heads. This observation motivated us to consider various mechanisms of coordination.

To understand the role of coordination in dynein function, we considered kinetic models of increasing complexity (see Figs. 3, 5, and 6). These investigations suggested two conceptually different coordination scenarios: one in which both heads can be in the same chemomechanical state and one in which such states are avoided. Only the second scenario guarantees that the motor moves with a predominantly "hand-over-hand" motion because in the first case when the heads are in identical states there is no bias for which head undergoes the next transition. One way to achieve a model in which chemically identical states (diagonal elements in the state matrix) are avoided is if the transition rates for the power stroke and ADP release depend on the chemical state of the other head. In particular, the rate of the power stroke should increase when the second head is detached from the MT, while ADP release from the rear head is accelerated when the heads are both associated with the MT at adjacent binding sites (i.e., separated by 8.2 nm). The first assumption seems reasonable because if the second head is detached, it does not impede the movement of the head undergoing the power stroke. The second assumption is plausible because the close proximity of the two heads when they occupy adjacent binding sites makes a physical interaction probable (Fig. 4). Given the feasibility of these assumptions, we performed a mathematical analysis to characterize the biophysical behavior of the model.

With the coordination described above, the model reproduced experimental measurements for both the velocity and run length. Our analysis revealed that coordination between the heads must accelerate the ADP-release and power-stroke rates by at least factors of 10^3. We consider this factor to be reasonable as it produces values for the two rates similar to those for the other biochemical steps in the hydrolysis cycle for a single head (see Figs. 8 and 9). We also explored the sensitivity of the motor's performance to variations in the ATP and Pi concentrations. In addition to the expected dependence of the motor's velocity on these concentrations,

they more strongly affected motor processivity. This behavior can be understood in terms of the effective rates for progression through the chemomechanical cycle and detachment from the MT. Indeed, while increasing the ATP concentration increases the effective forward rate and decreases detachment rate (Fig. 13), increasing Pi concentration decreases both rates such that the effective hydrolysis rate eventually becomes smaller than the detachment rate (Fig. 12).

The additional ATP-binding sites of the motor found in the AAA2–AAA4 subunits may contribute to the coordination of the heads by regulating rate-limiting steps. In particular, an effect similar to the one observed by modulating the Pi concentration also occurs if ATP hydrolysis by these sites causes a change in the affinity of the motor for the MT. If the probability that the heads dissociate from the MT decreases, then the run length of the motor increases. This behavior is consistent with the experimental results of Cho *et al.* who used mutagenesis to disrupt ATP hydrolysis at the AAA4 site.[18] They observed that dimers of the genetically altered motor were twice as processive as wild-type dynien. It is possible that ATP hydrolysis at the AAA4 site regulates the ADP-release rate e_1 from the primary site of the attached head in the noncompact conformation. Reduction in this rate slightly decreases the velocity but strongly increases the run length (see Fig. 10) in agreement with the observations by Cho *et al.* Another possibility is that the AAA3 site contributes to the second coordination mechanism. If disruption of this site leads to a slowing down of the power-stroke rate p_1, this would account for the reduction in the velocity and the run length (Fig. 8), as well as force generation as observed experimentally.[18]

Because we focused on mechanisms of coordination, our model was built on the idealization that the motor only takes steps of 8.2 nm. Our model is easily extended to allow for multiple step sizes. The key element of the mechanism of coordination that we suggest is the formation of a compact conformation in which the heads physically interact (see Fig. 4 and Ref. 10). Allowing for occasional larger steps (16.4 and 24.6 nm) creates the opportunity of disrupting the coordination between the heads and enriching the motor's behavior with "mis-stepping," such as backsteps or "inch worming." Conversely, because our proposed mechanism of coordination involves a physical interaction of the heads, any perturbation that disrupts this coordination should also change the step size distribution. This observation can potentially explain the efficacy of dynein in overcoming obstacles and navigating through the crowded environment by balancing small tightly coordinated steps with the larger more flexible ones. Finally, we note that our analysis did not consider the affects of an applied load on the full model. Including this effect can be accomplished using the same approach as was employed for the simple model for motor stepping in the absence of ATP. These and other extensions of our model will allow a quantitative comparison with the full range of available experimental data and is the focus of ongoing research.

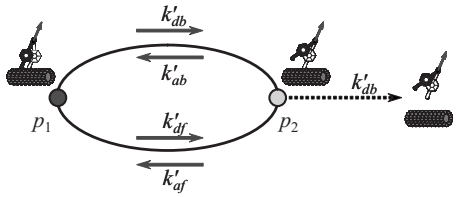

FIG. 14. A two-state model with detachment for force-induced stepping in the absence of ATP.

ACKNOWLEDGMENTS

We would like to acknowledge support from the following grants: NIH Grant Nos. R01-GM079271 and R01-HL077546 (D.T. and T.C.E.) and the American Heart Association, predoctoral Grant No. 0715215U (A.W.R.S.).

APPENDIX A: DERIVATIONS OF THE ATP-INDEPENDENT STEPPING MODEL

Let us denote the probability that at time t the motor is in the state (i) as $p_i(t)$ for $i=1,2$; then the master equations for the model in Fig. 14, which is equivalent to Fig. 2(a) in Sec. III, can be written as

$$\partial p_1 = -(k'_{db}+k'_{df})p_1 + (k'_{ab}+k'_{af})p_2,$$
$$\partial p_2 = -(k'_{ab}+k'_{af}+k'_{db})p_2 + (k'_{db}+k'_{df})p_1, \tag{A1}$$

where $p_1(t=0)=0$, $p_2(t=0)=1$, and $p_i(t\to\infty)=0$.

The mean time that the motor spends in state (i) prior to dissociation from the MT is $\tau_i=\int_0^\infty p_i(t)dt$, so that the mean run time (first-passage time) is $\langle\tau\rangle=\tau_1+\tau_2$.

Integrating Eq. (A1) yields

$$0 = -(k'_{db}+k'_{df})\tau_1 + (k'_{ab}+k'_{af})\tau_2,$$
$$-1 = -(k'_{ab}+k'_{af}+k'_{db})\tau_2 + (k'_{db}+k'_{df})\tau_1, \tag{A2}$$

and hence $\tau_1=(k'_{af}+k'_{ab})/k'_{db}(k'_{db}+k'_{df})$, $\tau_2=1/k'_{db}$ and

$$\langle\tau\rangle = \frac{k'_{db}+k'_{df}+k'_{af}+k'_{ab}}{k'_{db}(k'_{db}+k'_{df})}. \tag{A3a}$$

Similarly, the mean probability fluxes along the forward cycle are defined as $\pi_{ij}=\int_0^\infty[(\text{forward rate})_{ij}p_i - (\text{backward rate})_{ji}p_j]dt$ and given by

$$\pi_{12} = k'_{db}\tau_1 - k'_{ab}\tau_2 = \frac{k'_{db}k'_{af}-k'_{df}k'_{ab}}{k'_{db}(k'_{db}+k'_{af})},$$

$$\pi_{21} = k'_{af}\tau_2 - k'_{df}\tau_1 = \frac{k'_{db}k'_{af}-k'_{df}k'_{ab}}{k'_{db}(k'_{db}+k'_{df})} = \pi_{12} \equiv \pi,$$

$$\pi_{\text{out}} = k'_{db}\tau_2 = 1 = \pi_{\text{in}}.$$

Finally, we find that

$$\langle l\rangle = \pi\Delta x = \Delta x\frac{k'_{db}k'_{af}-k'_{df}k'_{ab}}{k'_{db}(k'_{db}+k'_{df})},$$
$$\langle V\rangle = \langle l\rangle/\langle\tau\rangle = \Delta x\frac{k'_{db}k'_{af}-k'_{df}k'_{ab}}{k'_{db}+k'_{df}+k'_{af}+k'_{ab}}. \tag{A3}$$

APPENDIX B: DERIVATIONS OF THE EFFECTIVE KINETICS RATES AND DISTRIBUTIONS

Let the probability of being at site n at time t be denoted as $q_n(t)$; then this function must satisfy the master equation $dq_n/dt=-(u_{\text{eff}}+w_{\text{eff}}+d_{\text{eff}})q_n+u_{\text{eff}}q_{n-1}+w_{\text{eff}}q_{n+1}$, with the initial condition $q_n(0)=\delta_{n,0}$. The probability to detach from the site n is $\rho(n)=\int_0^\infty d_{\text{eff}}q_n(t)dt=d_{\text{eff}}\tau_n$, where τ_n is the solution of the integrated master equation

$$(u_{\text{eff}}+w_{\text{eff}}+d_{\text{eff}})\tau_n-u_{\text{eff}}\tau_{n-1}-w_{\text{eff}}\tau_{n+1}=\delta_{n,0} \tag{B1}$$

and can be written in the form

$$\tau_n=AB^n \tag{B2}$$

subject to the normalization condition

$$\sum_{n=-\infty}^{+\infty}\tau_n=T=1/d_{\text{eff}}. \tag{B3}$$

Substituting Eq. (B2) into Eq. (B1) we obtain

$$w_{\text{eff}}B^2-(u_{\text{eff}}+w_{\text{eff}}+d_{\text{eff}})B+u_{\text{eff}}=0, \tag{B4}$$

and hence

$$B_{1,2}=\frac{(u_{\text{eff}}+w_{\text{eff}}+d_{\text{eff}})\mp\sqrt{(u_{\text{eff}}+w_{\text{eff}}+d_{\text{eff}})^2-4u_{\text{eff}}w_{\text{eff}}}}{2w_{\text{eff}}}. \tag{B5}$$

The physically relevant solution must satisfy the condition $\lim_{n\to\pm\infty}(\tau_n)=0$.

Therefore,

$$\tau_n=\mathrm{A}\times\begin{cases}B_1^n & \text{for } n=0,1,2,\ldots\\ B_2^n & \text{for } n=0,-1,-2,\ldots.\end{cases} \tag{B6}$$

Substituting the above expression into Eq. (B3), we find that

$$\begin{aligned}\sum_{n=-\infty}^{+\infty}\tau_n&=\sum_{n=0}^{+\infty}\tau_n+\sum_{n=0}^{+\infty}\tau_{-n}-\tau_0\\&=A\left(\sum_{n=0}^{+\infty}B_1^n+\sum_{n=0}^{+\infty}(1/B_2)^n-1\right)\\&=A\left(\frac{B_1}{1-B_1}+\frac{B_2}{B_2-1}\right)=\frac{1}{d_{\text{eff}}},\end{aligned} \tag{B7}$$

and finally,

$$A=\frac{1}{\sqrt{(u_{\text{eff}}+w_{\text{eff}}+d_{\text{eff}})^2-4u_{\text{eff}}w_{\text{eff}}}}. \tag{B8}$$

In the special case $w_{\text{eff}}=0$, the motor never reaches $n<0$, so that

$$B_2=+\infty,\quad B_1=B=\frac{u_{\text{eff}}}{u_{\text{eff}}+d_{\text{eff}}},\quad A=\frac{1}{u_{\text{eff}}+d_{\text{eff}}} \tag{B9}$$

and

$$\tau_n=\begin{cases}\dfrac{1}{u_{\text{eff}}+d_{\text{eff}}}\left(\dfrac{u_{\text{eff}}}{u_{\text{eff}}+d_{\text{eff}}}\right)^n & \text{for } n=0,1,2,\ldots\\ 0 \quad \text{for } n=0,-1,-2,\ldots.\end{cases} \tag{B10}$$

Furthermore, if w_{eff} is small ($\ll u_{\text{eff}}$), we can write the distribution of run lengths as

$$\begin{aligned}\rho(L)&=\rho(n\Delta x)\\&\approx d_{\text{eff}}Ae^{-(L/\Delta x)\ln(1/\mathrm{B})}\\&=\frac{d_{\text{eff}}}{u_{\text{eff}}+d_{\text{eff}}}e^{-(L/\Delta x)\ln(1+d_{\text{eff}}/u_{\text{eff}})}+O\left(\frac{w_{\text{eff}}}{u_{\text{eff}}}\right),\end{aligned} \tag{B11}$$

where

$$A=\frac{1}{u_{\text{eff}}+d_{\text{eff}}}+O\left(\frac{w_{\text{eff}}}{u_{\text{eff}}}\right),\quad B=\frac{u_{\text{eff}}}{u_{\text{eff}}+d_{\text{eff}}}+O\left(\frac{w_{\text{eff}}}{u_{\text{eff}}}\right). \tag{B12}$$

The mean run length is

$$\langle L\rangle=\Delta x(\pi_f-\pi_b)=\Delta x\frac{u_{\text{eff}}-w_{\text{eff}}}{d_{\text{eff}}}, \tag{B13}$$

which is consistent with the estimation obtained using Eq. (B11),

$$\begin{aligned}\langle L\rangle&\approx\Delta x\frac{\sum_{n=0}^{\infty}n\rho(n)}{\sum_{n=0}^{\infty}\rho(n)}\\&=\Delta x\frac{\sum_{n=0}^{\infty}n\mathrm{B}^n}{\sum_{n=0}^{\infty}\mathrm{B}^n}=\frac{\Delta x\mathrm{B}}{1-\mathrm{B}}\approx\Delta x\frac{u_{\text{eff}}}{d_{\text{eff}}}+O\left(\frac{w_{\text{eff}}}{u_{\text{eff}}}\right).\end{aligned} \tag{B14}$$

Finally, the expressions for the effective rates in terms of the probabilities for the states shown in Fig. 6 are

$$\begin{aligned}u_{\text{eff}}=\frac{\pi_f}{T}=\frac{u_{4A\to 1A}}{T}\Bigg(&\int_0^\infty p_{3B,\ 4A}dt+\int_0^\infty p_{3A,\ 4A}dt\\&+\int_0^\infty p_{4A,\ 4A}dt+\int_0^\infty p_{4A,\ 3B}dt+\int_0^\infty p_{4A,\ 3A}dt\\&+\int_0^\infty p_{4A,\ 4A}dt\Bigg),\end{aligned}$$

$$\begin{aligned}w_{\text{eff}}=\frac{\pi_b}{T}=\frac{w_{1A\to 4A}}{T}\Bigg(&\int_0^\infty p_{1A,\ 3B}dt+\int_0^\infty p_{1A,\ 3A}dt\\&+\int_0^\infty p_{1A,\ 4A}dt+\int_0^\infty p_{3B,\ 1A}dt+\int_0^\infty p_{3A,\ 1A}dt\\&+\int_0^\infty p_{4A,\ 1A}dt\Bigg),\end{aligned}$$

$$d_{\text{eff}} = \frac{\pi_d}{T} = \frac{u_{4A\to 1A}}{T}\left(\int_0^\infty p_{1A,\ 4A}dt + \int_0^\infty p_{1B,\ 4A}dt + \int_0^\infty p_{2B,\ 4A}dt + \int_0^\infty p_{4A,\ 1A}dt + \int_0^\infty p_{4A,\ 1B}dt + \int_0^\infty p_{4A,\ 2B}dt\right) + \frac{w_{3B\to 2B}}{T}\left(\int_0^\infty p_{1A,\ 3B}dt + \int_0^\infty p_{1B,\ 3B}dt + \int_0^\infty p_{2B,\ 3B}dt + \int_0^\infty p_{3B,\ 1A}dt + \int_0^\infty p_{3B,\ 1B}dt + \int_0^\infty p_{3B,\ 2B}dt\right),$$

where $u_{4A\to 1A}$ is the forward rate between states $(4A)$ and $(1A)$, while $w_{1A\to 4A}$ and $w_{3B\to 2B}$ are the backward rates between states $(1A)$ and $(4A)$ and $(3B)$ and $(2B)$, respectively.

[1] G. Mocz and I. R. Gibbons, Structure (London) **9**, 93 (2001).
[2] N. Mizuno, A. Narita, T. Kon, K. Sutoh, and M. Kikkawa, Proc. Natl. Acad. Sci. U.S.A. **104**, 20832 (2007).
[3] A. W. Serohijos, Y. Chen, F. Ding, T. C. Elston, and N. V. Dokholyan, Proc. Natl. Acad. Sci. U.S.A. **103**, 18540 (2006).
[4] S. L. Reck-Peterson and R. D. Vale, Proc. Natl. Acad. Sci. U.S.A. **101**, 1491 (2004).
[5] I. R. Gibbons, A. Lee-Eiford, G. Mocz, C. A. Phillipson, W. J. Tang, and B. H. Gibbons, J. Biol. Chem. **262**, 2780 (1987).
[6] I. R. Gibbons, B. H. Gibbons, G. Mocz, and D. J. Asai, Nature (London) **352**, 640 (1991).
[7] T. Kon, M. Nishiura, R. Ohkura, Y. Y. Toyoshima, and K. Sutoh, Biochemistry **43**, 11266 (2004).
[8] K. Imamula, T. Kon, R. Ohkura, and K. Sutoh, Proc. Natl. Acad. Sci. U.S.A. **104**, 16134 (2007).
[9] R. Lipowsky and S. Liepelt, J. Stat. Phys. **130**, 39 (2007).
[10] S. L. Reck-Peterson, A. Yildiz, A. P. Carter, A. Gennerich, N. Zhang, and R. D. Vale, Cell **126**, 335 (2006).
[11] E. L. Holzbaur and K. A. Johnson, Biochemistry **28**, 7010 (1989).
[12] T. Mogami, T. Kon, K. Ito, and K. Sutoh, J. Biol. Chem. **282**, 21639 (2007).
[13] T. Kon, T. Mogami, R. Ohkura, M. Nishiura, and K. Sutoh, Nat. Struct. Mol. Biol. **12**, 513 (2005).
[14] P. Hook, A. Mikami, B. Shafer, B. T. Chait, S. S. Rosenfeld, and R. B. Vallee, J. Biol. Chem. **280**, 33045 (2005).
[15] S. A. Burgess, M. L. Walker, H. Sakakibara, P. J. Knight, and K. Oiwa, Nature (London) **421**, 715 (2003).
[16] N. Numata, T. Kon, T. Shima, K. Imamula, T. Mogami, R. Ohkura, K. Sutoh, and K. Sutoh, Biochem. Soc. Trans. **36**, 131 (2008).
[17] A. Silvanovich, M. G. Li, M. Serr, S. Mische, and T. S. Hays, Mol. Biol. Cell **14**, 1355 (2003).
[18] C. Cho, S. L. Reck-Peterson, and R. D. Vale, J. Biol. Chem. **283**, 25839 (2008).
[19] Y. Takahashi, M. Edamatsu, and Y. Y. Toyoshima, Proc. Natl. Acad. Sci. U.S.A. **101**, 12865 (2004).
[20] R. Mallik, B. C. Carter, S. A. Lex, S. J. King, and S. P. Gross, Nature (London) **427**, 649 (2004).
[21] S. Toba, T. M. Watanabe, L. Yamaguchi-Okimoto, Y. Y. Toyoshima, and H. Higuchi, Proc. Natl. Acad. Sci. U.S.A. **103**, 5741 (2006).
[22] R. Mallik, D. Petrov, S. A. Lex, S. J. King, and S. P. Gross, Curr. Biol. **15**, 2075 (2005).
[23] B. M. Paschal, H. S. Shpetner, and R. B. Vallee, J. Cell Biol. **105**, 1273 (1987).
[24] J. F. Presley, N. B. Cole, T. A. Schroer, K. Hirschberg, K. J. Zaal, and J. Lippincott-Schwartz, Nature (London) **389**, 440 (1997).
[25] S. J. King and T. A. Schroer, Nat. Cell Biol. **2**, 20 (2000).
[26] Z. Wang, S. Khan, and M. P. Sheetz, Biophys. J. **69**, 2011 (1995).
[27] A. Gennerich, A. P. Carter, S. L. Reck-Peterson, and R. D. Vale, Cell **131**, 952 (2007).
[28] A. B. Kolomeisky and M. E. Fisher, Physica A **279**, 1 (2000).
[29] D. M. Goedecke and T. C. Elston, J. Theor. Biol. **232**, 27 (2005).
[30] D. Tsygankov and M. E. Fisher, J. Chem. Phys. **128**, 015102 (2008).
[31] M. E. Porter and K. A. Johnson, J. Biol. Chem. **258**, 6582 (1983).
[32] E. L. Holzbaur and K. A. Johnson, Biochemistry **25**, 428 (1986).
[33] K. A. Johnson, J. Biol. Chem. **258**, 13825 (1983).
[34] T. Shimizu, S. P. Marchese-Ragona, and K. A. Johnson, Biochemistry **28**, 7016 (1989).
[35] T. Shimizu, T. Katsura, P. L. Domanico, S. P. Marchese-Ragona, and K. A. Johnson, Biochemistry **28**, 7022 (1989).
[36] E. L. Holzbaur and K. A. Johnson, Biochemistry **28**, 5577 (1989).
[37] K. Kikushima, T. Yagi, and R. Kamiya, FEBS Lett. **563**, 119 (2004).